Geobiology (2007), 5, 219–234 DOI: 10.1111/j.1472-4669.2007.00113.x

Chemical reactivity of microbe and mineral surfaces in hydrous ferric oxide depositing hydrothermal springs

S. V. LALONDE,[1] L. AMSKOLD,[1] T. R. MCDERMOTT,[2] W. P. INSKEEP[2] AND K. O. KONHAUSER[1]

[1]*Department of Earth and Atmospheric Sciences, University of Alberta, Edmonton, Alberta, Canada T6G 2E3 and*
[2]*Department of Land Resources and Environmental Sciences, Montana State University, Bozeman, Montana 59717, USA*

ABSTRACT

The hot springs in Yellowstone National Park, USA, provide concentrated microbial biomass and associated mineral crusts from which surface functional group (FG) concentrations and pK_a distributions can be determined. To evaluate the importance of substratum surface reactivity for solute adsorption in a natural setting, samples of iron-rich sediment were collected from three different springs; two of the springs were acid-sulfate-chloride (ASC) in composition, while the third was neutral-chloride (NC). At one of the ASC springs, mats of S°-rich *Hydrogenobaculum*-like streamers and green *Cyanidia* algae were also collected for comparison to the sediment. All samples were then titrated over a pH range of 3–11, and comparisons were made between the overall FG availability and the concentration of solutes bound to the samples under natural conditions. Sediments from ASC springs were composed of hydrous ferric oxides (HFO) that displayed surface FGs typical of synthetic HFO, while sediments from the NC spring were characterized by a lower functional group density, reflected by decreased excess charge over the titration range (i.e., lower surface reactivity). The latter also showed a lower apparent point of zero charge (PZC), likely due the presence of silica (up to 78 wt. %) in association with HFO. Variations in the overall HFO surface charge are manifest in the quantities and types of solutes complexed; the NC sediments bound more cations, while the ASC sediments retained significantly more arsenic, presumably in the form of arsenate ($H_2AsO_4^-$). When the microbial biomass samples were analyzed, FG concentrations summed over the titratable range were found to be an order of magnitude lower for the S°-rich mats, relative to the algal and HFO samples that displayed similar FG concentrations on a dry weight basis. A diffuse-layer surface complexation model was employed to further illustrate the importance of surface chemical parameters on adsorption reactions in complex natural systems.

Accepted: 16 April 2007; Submitted: 7 November 2006

Corresponding author: S. V. Lalonde. Tel. 780-492-6532; Fax: 780-492-2030; e-mail: stefan.lalonde@ualberta.ca.

INTRODUCTION

Chemical reactions occurring at the solid-water interface, including adsorption, ion-exchange, hydrolysis, precipitation, polymerization, oxidation–reduction, and dissolution, are dependent upon the surface charge characteristics of the submerged substratum (Davis and Kent, 1990). Surface charge, in turn, is determined by the properties and concentrations of chemical functional groups (FGs) exposed to the aqueous environment. Some minerals, such as micas, zeolites, and clay minerals, possess permanent structural surface charges resulting from cationic substitution within their crystal lattice, while others, such as metal oxyhydroxides and complex organic macromolecules, develop charge solely as the result of surface functional group protonation/deprotonation reactions (Langmuir, 1997). For example, the typical negative charge associated with the cell walls and extracellular layers of microorganisms develops as a function of pH, primarily via the following four functional group deprotonation reactions:

$$\text{R-COOH} \rightarrow \text{R-COO}^- + \text{H}^+ \quad (1)$$

$$\text{R-PO}_4\text{H}_2 \rightarrow \text{R-PO}_4\text{H}^- + \text{H}^+ \quad (2)$$

$$\text{R-NH}_3^+ \rightarrow \text{R-NH}_2 + \text{H}^+ \quad (3)$$

$$\text{R-OH} \rightarrow \text{R-O}^- + \text{H}^+ \quad (4)$$

where R represents a microbial surface. Reactions (1) and (2) proceed spontaneously at neutral pH, and the deprotonated ligands are responsible for the bulk of the overall negative cell

surface charge typical at pH values greater than ~3 (Bayer and Sloyer, 1990). Reaction (3) occurs at pH values between 8–11 (Hunt, 1986), and reaction (4) only becomes significant at pH values around 11 (Martell and Smith, 1989), thus negligibly affecting microbial surface charge under most conditions. These functional groups also act as efficient ligands for the complexation of various cations and as nucleation sites for a variety of authigenic mineral phases (see Konhauser, 2007 for details). Importantly, the large surface area-to-volume ratios of most microorganisms, their ubiquity in the environment, and in many cases their high population densities, make them extremely important agents in biogeochemical cycles, particularly with respect to elemental partitioning.

Many minerals also possess highly reactive surfaces that exert control over the chemistry of solutions with which they are in contact. Hydrous ferric oxides have received significant attention due to their widespread occurrence and high sorptive capacity; indeed, numerous HFOs have been studied as model surfaces for surface complexation reactions (e.g., Dzombak and Morel, 1990). HFOs are poorly ordered minerals with relatively large surface area (Roden, 2003), and are dominated by hydroxyl surface functional groups (e.g., Smith and Ferris, 2001). Such minerals have been shown to precipitate rapidly in environments where Fe(II)-bearing waters come into contact with O_2 at pH > 4. Microorganisms are often implicated in HFO formation, playing either a completely passive role, i.e., becoming covered by abiological precipitates; facilitating mineral nucleation by providing ligands to adsorb dissolved Fe species; or an active role, by causing mineral precipitation through their metabolic oxidation of Fe(II) (Konhauser, 1998).

Solute adsorption to a biological or mineral surface is dictated by the structural and compositional nature of the exposed functional groups, as well as the unique physicochemical properties of each sorbate forming a surface complex. Spectroscopic methods, such as Fourier transform infrared spectroscopy (FTIR), X-ray absorption near edge structure (XANES), X-ray absorption fine structure (XAFS), and electron energy loss spectroscopy (EELS), can provide detailed information regarding the identity and coordination environment of a surface complex. However, they are unable to provide quantitative estimates regarding the availability (in terms of concentration) of different surface sites (e.g., functional groups) where adsorption reactions may occur; in other words, the chemical reactivity of the surface in question. The latter, though, can be readily assessed by potentiometric titration, where the deprotonation of surface FGs can be quantified as a function of pH. To this data, concentrations and proton stability constants (also known as acidity constants, or K_a) of discrete surface FG sites may be fitted for bacterial (e.g., Fein *et al.*, 1997; Cox *et al.*, 1999) and mineral surfaces (e.g., Kennedy *et al.*, 2003; Smith and Ferris, 2003). It should be noted that a single so-called 'discrete' site actually represents a mean of compounds that possess a similar FG. The result is a set of chemical parameters quantitatively describing a surface, which may be extrapolated to predict interactions between this surface and competing aqueous species in complex solutions, i.e., using surface complexation models (e.g., Fein *et al.*, 2001).

One motivation for modelling microbial and mineral surface chemistry is that it has wide-ranging implications for solute sorption and biomineralization reactions. For instance, understanding the effectiveness of reactive surfaces in 'fixing' toxic metal cations from solution is vital in constructing accurate contaminant transport models, and ultimately designing effective bioremediation strategies (e.g., Bethke and Brady, 2000). Yet this is where significant gaps in our current level of understanding exist. Microbial surface reactivity and solute sorption models have, to date, mostly been based on axenic laboratory cultures where cells are harvested at optimal growth conditions, the surface polymers (extracellular polysaccharides (EPS), sheaths, S-layers) may be chemically removed, and the cells may be acid-washed to strip off any cations previously adsorbed to their surfaces (e.g., Yee and Fein, 2001). Despite those studies resolving the capacity of biomass to sorb solutes from solution, they have not yet considered (1) the chemical reactivity of different species growing as part of a complex, mixed microbial community with cells in different growth phases held together by extracellular layers; and (2) the chemical or biological effects that natural, multi-element fluids might have on the charge characteristics of microbial surfaces. Furthermore, the adsorptive properties of microbes living in natural systems are poorly understood, as separation of microbial and mineral components for individual investigation is fraught with difficulty. In fact, as far as we are aware, only the study of Kennedy *et al.* (2003) has examined natural mineral–microbe assemblages with the view of measuring the surface reactivity of the composites.

The goal of this preliminary study is to quantify and compare the sorptive properties of the individual microbial and mineral components in a natural microbial ecosystem. We selected geochemically diverse hydrothermal springs in Yellowstone National Park, USA, on the basis of well-characterized biomass and the presence of highly reactive iron oxide minerals (HFO). Notably, these particular HFOs are known for their high arsenic content (Lagner *et al.*, 2001; Inskeep *et al.*, 2004), which approach experimental upper limits for arsenic content in synthetic HFO phases (Waychunas *et al.*, 1993). We report functional group concentrations and proton stability constants for the surfaces of HFO from three different springs, and then compare the HFO from one of those springs to the biomass of thermophilic bacteria and algae collected from the same spring. We also measured the concentrations of solutes complexed to these surfaces, and for the HFO samples, applied a diffuse-layer surface complexation model (SCM) to evaluate the predictive ability of the reported surface parameters to describe the nature and extent of sorptive processes occurring on the mineral surface. In doing so, we highlight some of the

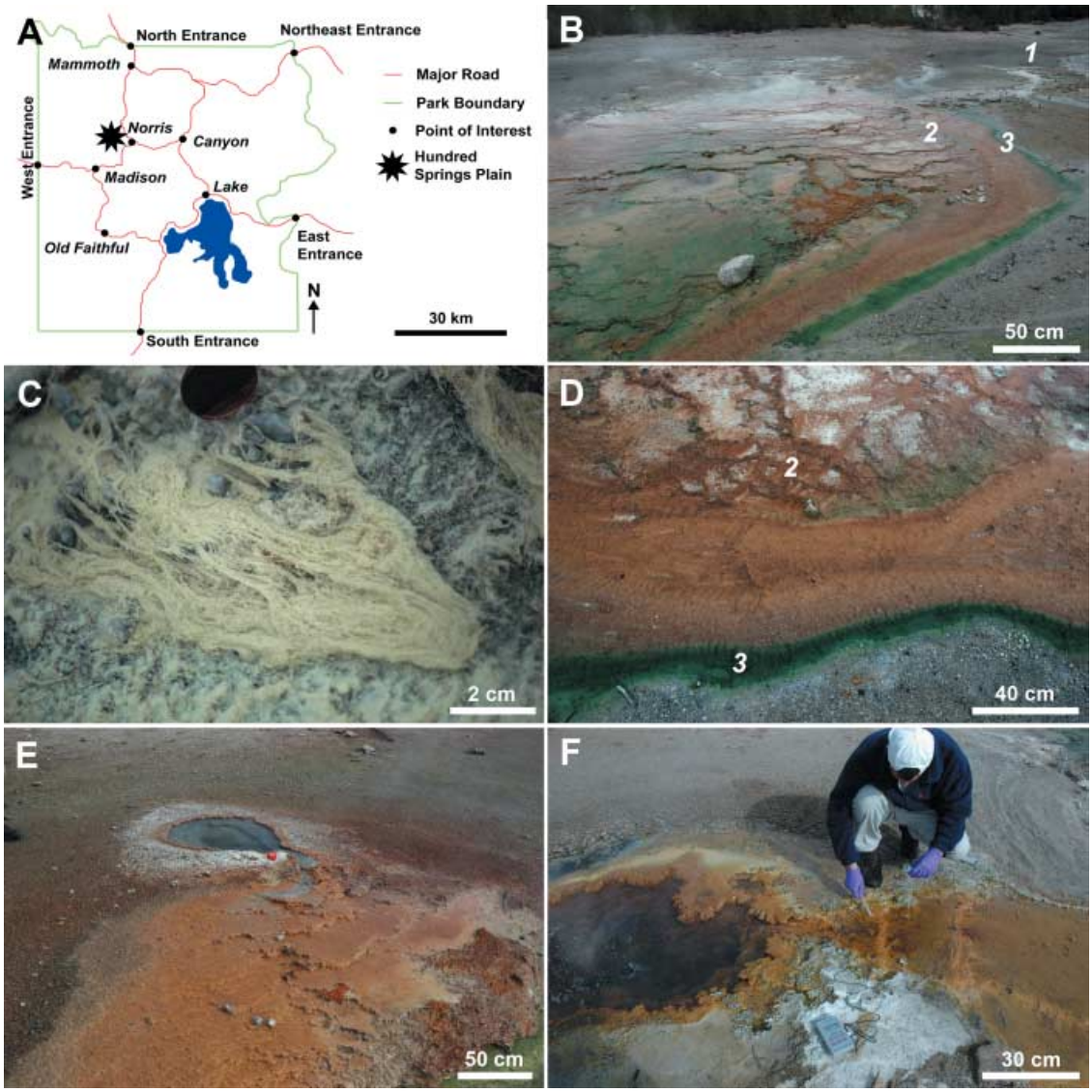

Fig. 1 (A) Map of sampling locations in Norris Geyser Basin, Yellowstone National Park. (B) Overview of Beowulf Spring, with close up of (C) 'yellow mat' [labelled 1 in (B)] consisting of thermophilic, filamentous bacteria and elemental sulfur precipitates and (D) the sharp transition zone between the hydrous ferric oxide (HFO) (label 2) and the green mat of *Cyanidia* algae (label 3). (E) Gap spring, where terraced HFO mats accumulate within the outflow surrounding the vent. (F) Perpetual Spouter, similarly showing HFO deposition within the outflow channel.

advantages and disadvantages of applying surface chemical characterization techniques to natural samples that comprise mixtures of microbial and mineral components.

Previous Work at Study Area

The Hundred Springs Plain of Norris Basin (Fig. 1A) contains a variety of geothermal springs. Some are classified as acid-sulfate-chloride (ASC), which are characterized by low pH, and typically contain high concentrations of reduced chemical species, including H_2, H_2S, As(III) and Fe(II), at discharge (Ball *et al.*, 2002; Langner *et al.*, 2001). Also found are neutral-chloride (NC) springs, which have similar geochemistry, but higher pH. In this study, we sampled two ASC springs (Beowulf and Gap Spring) and one NC spring, Perpetual Spouter.

Of the three springs, Beowulf Spring has been the subject of recent aqueous, biological, and mineralogical investigations. It is home to microbial mat communities that vary compositionally with distance down the outflow channel (Fig. 1B), correlating with major changes in temperature and aqueous/solid phase geochemistry (Langner *et al.*, 2001; Inskeep *et al.*, 2004). Those authors reported that vent waters contain abundant dissolved Fe(II) (49.3 μM, with a $Fe(II)/Fe_{total}$ ratio of 0.91 to 0.94), As(III) (23.9 μM), and H_2S (80 μM). The concentration of dissolved H_2S then declines to below 6 μM at 9 m, presumably due to a combination of degassing and

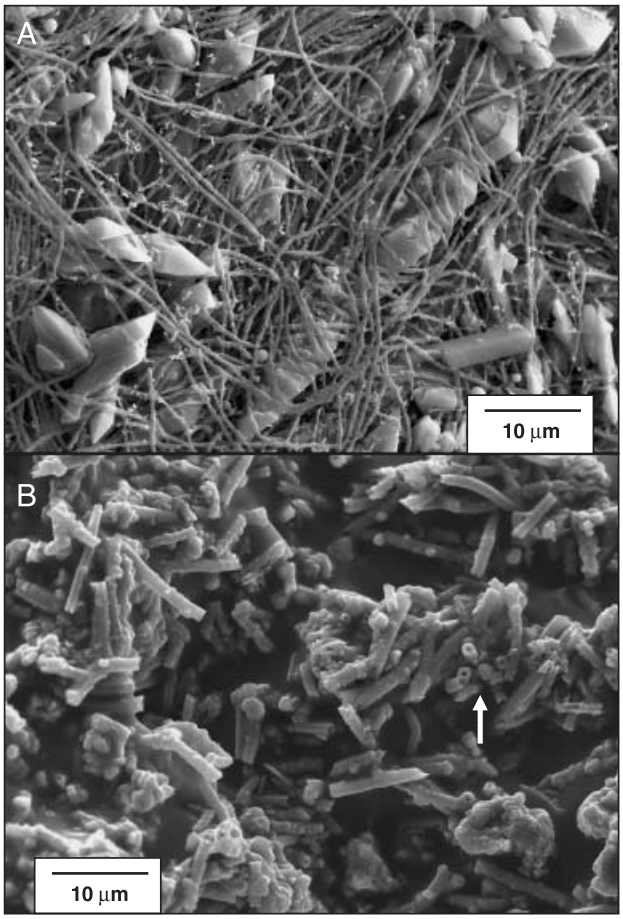

Fig. 2 Scanning electron micrographs (SEM) of filamentous microorganisms from Beowulf Spring associated with S^0-rich mats (A) or encrusted with high As-rich, hydrous ferric oxide (HFO) precipitates (B). SEM image of Fe-encrusted cells (see arrow). See Langner *et al.* (2001) and Inskeep *et al.* (2004) for SEM procedures.

oxidation, resulting in the precipitation of elemental sulfur (as determined by EDX; Langner *et al.*, 2001) that ranges from amorphous to well-crystalline rhombohedral structures (Fig. 1C; Fig. 2A). In conjunction with filamentous microorganisms that form visible streamers, the solid-phase S° forms a yellow mat. Molecular analyses of the yellow mats demonstrated the presence of numerous *Hydrogenobaculum*-like populations, and that archaeal phylotypes were conspicuously absent at this location (Jackson *et al.*, 2001). No As(III) oxidation was observed within the S° depositional zone (0–3 m), nor was any As(III) or As(V) sequestered within this zone. However, at downstream locations where H_2S is absent, microbial oxidation of As(III) to As(V) occurred at rates faster than ever reported for natural waters. These reactions are associated with an iron-depositing zone (Fig. 1D), composed of an electron and X-ray amorphous HFO phase with 0.6–0.7 mole ratio As(V):Fe(III) (with arsenate, $H_2AsO_4^-$, adsorbed as a bidentate complex), among the highest As contents observed in naturally occurring HFOs (Morin *et al.*, 2003; Inskeep *et al.*, 2004). Close inspection of the HFOs revealed the presence of an extensive network of microorganisms (0.5 μm in diameter, and reminiscent in morphology to Fe(II)-oxidizing bacteria) with epicellular Fe(III) precipitates that suggest direct microbial templating of iron (Fig. 2B; Inskeep *et al.*, 2004). Numerous archaeal and bacterial species have been identified here, including those of the genera *Acidimicrobium*, *Thiomonas*, *Metallosphaera*, and *Marinithermus*; several of these cultured relatives are known Fe(II) and/or As(III) oxidizers (Inskeep *et al.*, 2004). These cells collectively yield approximately 1% organic carbon to the HFO (Inskeep *et al.*, 2004). The iron-depositing zone also contains *Hydrogenobaculum* populations. Donohoe-Christiansen *et al.* (2004) isolated an As(III)-oxidizing *Hydrogenobaculum* from a HFO-rich region in the ASC spring referred to Dragon Spring and showed that H_2S was a potent inhibitor of As(III) oxidation, suggesting the absence of As(III) oxidation activity in the yellow S°-rich mat zone may be due to the presence of high concentrations of H_2S.

High rates of As(III) oxidation were also observed in the adjacent green mats (Langner *et al.*, 2001) (Fig. 1D) that are characterized by a dense surface coverage of thermoacidophilic eukaryotic algae belonging to the order Cyanidiales (Seckbach, 1994). Interestingly, some portions of the green mats show significant concentrations of Fe and As, with elemental ratios identical to the HFOs.

METHODS

Aqueous sample collection

Spring waters (25 mL) were obtained by syringe and filtered through 0.22 μm in-line nylon syringe filters. Waters from Gap Spring (Fig. 1E) and Perpetual Spouter (Fig. 1F) were collected 1 m from the outflow with temperatures of 83 °C and 81 °C, respectively. At Beowulf Spring there are two sources (designated 'W' and 'E'), which mix 4–5 m downstream. Waters at Beowulf were collected at locations corresponding to the position of the yellow S^o-rich mats at Beowulf W (adjacent to the vent with temperature 55 °C), and a further 5 m below the mixing zone in association with the green algal mats and the HFO that form a well-defined thermal gradient of 44–51 °C (see Fig. 1B, D). Samples were acidified by TraceMetal grade HNO_3, stored in ice for transport, and immediately refrigerated upon return to the laboratory at Montana State University. Spring temperature and pH were measured in the field using a digital thermometer and an Orion Ross (#8165BN) pH meter calibrated between 2 and 4 for ASC springs and 4 and 10 for the NC spring.

Solid sample collection

HFO samples from all three springs were obtained from submerged microbial Fe-encrusted terraced structures using

a stainless steel scalpel. At Perpetual Spouter and Gap Spring, approximately 5 g of sample was obtained 1 m from the outflow. At Beowulf Spring, approximately 5 g of brown, HFO-mat composite was collected 5 m downstream from the mixing point of the West and East sources. In addition, at Beowulf, we sampled 1 g of the yellow, S°-rich mats found proximal to geothermal discharge in Beowulf West, and 1 g of green algal cells occupying the thermal gradient running parallel to the HFOs. All samples were stored in spring water for transport and refrigerated until analyses were complete within 48 h of sampling.

Acid-base titration

All glassware and plasticware were acid-washed in ~30% v/v concentrated HCl for a minimum of 30 min, following which they were soaked in deionized water for a minimum of 2 h. In an attempt to isolate microbial and mineral surfaces with minimal pH disturbance, samples were prepared at, and titrated from, the pH of the spring from which they were obtained. Samples from the two ASC springs (Beowulf, Gap) were prepared for titration by four alternating wash (10-s agitation followed by 10-min soak) and harvest (centrifugation at 11 050 *g* for 10 min) cycles using ~40 ml of 0.01 M KNO_3 titration electrolyte adjusted to pH ~3 with concentrated TraceMetal grade HNO_3. The HFO from Perpetual Spouter (NC type) was similarly prepared at pH ~7, and was titrated up and down from pH 7 to obtain a complete dataset for surface characterization. ASC samples were titrated up from pH ~3 to pH 11; however, additional samples of green algae were instead washed at pH ~11 and titrated down to pH 3 to evaluate pH-dependent effects of the preparation procedure.

For each individual titration, 0.06 to 0.5 g dry weight of washed sample was suspended in ~50 ml of fresh titration electrolyte in a 125-ml titration flask equipped with a pre-calibrated Ross-type pH electrode (Mandel Scientific, Guelph, Ontario, Canada), thermocouple, magnetic stir bar, titrant dispenser and N_2 purge line. Titrations were performed at 23 °C, either alkalimetrically to pH 11 with 0.01 M NaOH (Fisher-certified 0.01 M NaOH solution) or acidimetrically to pH 3 with 0.01 M HNO_3 prepared from TraceMetal grade HNO_3 and standardized against 0.01 M NaOH. A QC-Titrate autotitrator (Mandel Scientific) was interfaced to a personal computer and set to variably dispense titrant for increments of 0.1 pH units when electrode stabilities of 0.5 mV s^{-1} were achieved. Suspensions were purged with N_2 gas for 30 min prior to, and throughout, the titrations. Electrode calibrations using commercial buffers of pH 3.0, 4.0, 7.0, 10.0, and 12.0 were performed between every set of titration replicates (three to five) representing a single sample, and all pH measurements were automatically temperature-corrected. To satisfy the selected electrode stability criteria, and cover the pH range of interest, each titration took approximately 50 min. Following titration, selected samples were immediately titrated in the opposite direction to evaluate titration reversibility.

After the titrations, the sample material was collected by filtration onto pre-weighed 1.2 μm glass-fibre filters (GF/C no. 42, Whatman Inc., Florham Park, NJ, USA) and weighed after 7 days of air-drying in covered containers. This weight was subsequently used to normalize functional group concentrations; normalization on the basis of surface area was avoided because (1) surface area analysis by BET involves drying the sample, which may introduce additional error, especially with the biological samples, and (2) most studies on the surface reactivity of microorganisms report their results in terms of mass. In order to determine the concentrations of solutes sorbed under natural conditions, all solutions used for washing and titration were also filtered to 0.22 μm and then subsequently analyzed for selected aqueous species using a Quadrupole ICP-MS (Perkin Elmer Elan 6000, University of Alberta).

Discrete site modelling

In examining the titratible charges, three basic substrata were studied: HFOs, S°-rich mats, and green mats of *Cyanidia* cells. Due to the HFO encrustation of microbial cells in the iron-depositing zone, and the low organic C content (1%) of the HFO (recall Inskeep *et al.*, 2004), titratable charges associated with those samples were assumed to be dominated by the mineral precipitates associated with the microbial community, and not from microbial cell surface functional groups themselves. The green mat samples, however, are dominated by *Cyanidia* algae, and so consequently, we expect cell surface FGs (i.e. amino acids, carboxylic acids, some hydroxyl groups) to be most important, and indeed, dominate, proton exchange reactions.

A pK_a spectrum approach was employed to model mineral and biological functional group concentrations; possible FG acidity constants (expressed herein as log K_a, or pK_a) values are fixed in an interval (in this study 3–11, with increments of 0.2), and FG concentrations are iteratively optimized across the pK_a spectrum by linear programming until the best fit to measured excess charge is achieved (Brassard *et al.*, 1990). The charge balance of the system is first rearranged such that the surface charge arising from the deprotonation of discrete FGs may be expressed in terms of measured parameters (right-hand side of equation (5)):

$$\sum_{j=1}^{n} [L_j^-] - [ANC] = Cb_i - Ca_i + [H^+]_i - [OH^-]_i \quad (5)$$

where, for the i^{th} addition of titrant, Cb and Ca are the concentrations of base and acid, respectively; $[H^+]$ (and $[OH^-]$ by proxy) are monitored by the pH electrode; $[L_j^-]$ is the concentration of deprotonated FGs for the j^{th} monoprotic site of n possible sites set by the pK_a spectrum; and the acid-neutralizing capacity [ANC] is a constant offset representing the difference between FGs that remain protonated and those that deprotonate over the titration range (Smith and Ferris,

2001). By this arrangement, surface charge is assumed to arise solely from the deprotonation of FGs [left-hand side of equation (5)], i.e., the surface charge at any given pH is equal to either side of equation (5). At the initial pH of titration, the concentration of base is set to zero, and the concentration of acid is assumed to equal $[H^+] - [OH^-]$, so that surface charge is zero at initiation. This formalism does not affect the spectrum of modelled FG sites; the ANC term serves as a constant surface charge offset accounting for the zero initial charge assumption, from which the modelled FG site distribution is independent. The assumption of zero surface charge at titration initiation simply facilitates the presentation of surface charge excess plots (see Results).

FG concentration at each pK_a interval was fitted to the excess charge data by expressing the left-hand side of equation 5 in terms of the both protonated and deprotonated (total) sites (L_{Tj}):

$$\sum_{j=1}^{n} \frac{K_{aj}[L_{Tj}]}{[H^+]_i + K_{aj}} - [\mathrm{ANC}] = \mathrm{Cb}_i - \mathrm{Ca}_i + [H^+]_i - [OH^-]_i \quad (6)$$

Fitting was performed with the computer program MATLAB (version 6.5.1, The Mathworks, Inc., Natick, MA, USA) by linear programming (Brassard *et al.*, 1990), using a scripted implementation provided by D. Scott Smith (Wilfrid Laurier University). The pK_a spectrum modelling approach ignores pH-dependent charging effects on proton stability constants, and thus all pK_a values reported here are apparent, rather than intrinsic. Apparent point of zero charge (PZC), the pH value where the concentration of protonated and deprotonated FGs is equivalent (i.e., surface charge is zero), was calculated for each sample by finding the concentration-weighted pK_a mean of discrete sites; it is important to note that FGs not detected over the modelled range (pH 4–10) may lead to a significant discrepancy between the apparent and 'true' PZC. Diffuse-layer surface complexation modelling was applied to the three natural HFO surfaces using Visual MINTEQA2 (Gustafsson, 2000).

RESULTS

Stream geochemistry

Analyses of the three springs indicate very similar chemistry (Table 1), with the exception of pH and Fe. Both locations sampled at Beowulf (E and W) and Gap Spring have a pH around 3, while Perpetual Spouter has a neutral pH. Iron concentrations are an order of magnitude greater in Gap Spring than in Perpetual Spouter, at 79.0 μM and 2.7 μM, respectively. The Fe concentrations measured at Beowulf lie between these two values, at 34.6 and 38.7 μM for 'W' and 'E' sources, respectively.

Table 1 Values for pH, temperature and concentration of various elements (μM or nM) in aqueous samples taken at the same locations of solid phase samples. *concentrations from Inskeep (determined at Montana State University)

	Spring			
Analyte (μM)	Perpetual Spouter	Gap Spring	Beowulf West	Beowulf East
pH	7.0	3.3	3.0	3.1
Temperature (°C)	83.6	81	52.5	67
Na	19762.5	11759.1	11572.1	11135.8
Si*	5100	5300	4700	4700
K	1411.8	1028.2	1240.5	1225.1
B	1132.2	657.6	644.6	640.6
Li	944.3	454.0	544.4	537.4
Ca	274.8	87.4	127.9	124.5
As	40.4	30.2	18.7	19.6
Rb	5.7	2.9	3.8	3.8
Cs	4.7	2.0	2.7	2.6
Mg	3.4	10.3	8.5	8.2
Al	3.1	73.6	125.9	123.7
Fe	2.7	79.0	34.6	38.7
(nM)	Perpetual	Gap	Beowulf W	Beowulf E
Mn	805	810	564	546
Sr	457	182	242	239
Ba	134	1410	847	841
Be	91	208	114	124
Cu	142	88	82	82
Se	148	93	95	93
Zn	90	1297	455	873

Bulk composition of HFOs

The HFOs from Beowulf Spring have been previously characterized utilizing a suite of microscopic and spectroscopic methods (Inskeep *et al.*, 2004). Their high As content (As:Fe mole ratio = 0.62) is typical of other HFOs from acidic springs in Norris Geyser Basin, including the additional ASC spring used in this study, Gap Spring. Using XANES and EXAFS data, the same authors also concluded that arsenate is bound to Fe-octahedra via primarily bidentate binuclear surface complexes. The Fe cluster size was estimated to be only 40–80 atoms, based on complete surface coverage by arsenate. In contrast, the HFOs from Perpetual Spouter have a significantly different composition. First, the As content is very low, despite the fact that the aqueous arsenate concentration is higher than ASC spring waters (Table 1). Second, unlike the ASC HFOs, the HFOs found at Perpetual Spouter contain considerable Si; preliminary EDAX analyses show that the HFOs from the latter have a Si:Fe mole ratio of approximately 4.3:1 versus negligible Si content at Beowulf and Gap Spring (W. P. Inskeep, unpublished data). Further characterization of this phase is underway, and at this time it is difficult to ascertain relative contributions from particulate silicate mineral phases (e.g., quartz) versus authigenically precipitated amorphous silica versus HFO that has sorbed or co-precipitated significant amounts of silica. Given the high concentration of impurities, it is questionable as to whether or not the Fe-rich materials can

Table 2 Concentration of elements (μmol or nmol g^{-1} dry weight) desorbed from hydrous ferric oxide (HFO) and microbial samples. The last column is the difference in elements desorbed during titration of washed and unwashed *Cyanidia* mat material. Note: Iron concentrations are considered not applicable for HFO washing fluids

Analyte (μmol g^{-1})	Perpetual HFO	Gap HFO	Beowulf HFO	Beowulf YLW	Beowulf GRN
Mg	1300.5	1124.8	981.3	623.2	2111.6
Fe	NA	NA	NA	0.6	4.0
Al	14.8	0.6	0.5	0.8	1.8
As	0.5	79.8	56.7	1.4	121.1
(nmol g^{-1})	Perpetual	Gap	Beowulf HFO	Beowulf YLW	Beowulf GRN
B	4508	630	<500	1130	2880
Rb	4219	13	12	41	93
Cs	3187	5	7	1	8
Li	3006	10	16	54	40
Ca	1799	56	118	258	687
Mn	766	1	1	7	29
Ba	356	1	1	4	168
Sr	332	2	1	3	8
Zn	251	16	23	49	152
Cu	36	16	19	17	49

NA, not applicable. YLW, yellow mats. GRN, green mats.

actually be considered true HFO. It is not surprising that these natural HFO-like precipitates contain significant As and Si, given the highly reactive nature of HFO. Previous studies have shown that 0.5 mole ratio arsenic contents are not inconsistent with HFO, based on HFO surface reactivity (see Inskeep *et al.*, 2004 and references therein), and for the scope of this paper, we consider silica in the same context. Accordingly, in this study we employ the term 'HFO' until a more appropriate one may be defined.

Surface elemental concentrations

Elements concentrated on surfaces were determined by analyzing solutes desorbed during wash and titration procedures. For all HFO and biomass samples, Mg is universally found at the highest surface concentrations (Table 2). In the case of the HFOs, the surface concentrations of Al, Rb, Cs, Li, Ca, Mn, Ba, Sr, and Zn are all at least an order of magnitude greater at Perpetual Spouter than the ASC springs, while the concentration of As is considerably less. In terms of biomass (both of which were from Beowulf), the green *Cyanidia* mats consistently released higher concentrations of analyzed elements than the yellow S°-rich mats.

These patterns are similarly reflected by concentration factors, which allow for a quick evaluation of how elements are partitioned between the aqueous and the solid phases, with positive values indicating preferential accumulation on the solid relative to the effluent. For example, Mg was concentrated to the greatest extent by all samples (Figs 3 and 4). Furthermore, the HFO from Perpetual Spouter more strongly concentrated all elements than the ASC HFOs, with the exception of As and Cu (Fig. 3). Interestingly, the HFOs from Beowulf and Gap Spring showed almost identical patterns, despite having formed from different spring waters. In comparison with HFO from Beowulf, the biomass samples (both yellow and green mats) from Beowulf typically display higher concentration factors, with the green mats showing the greatest sorptive capacity (Fig. 4).

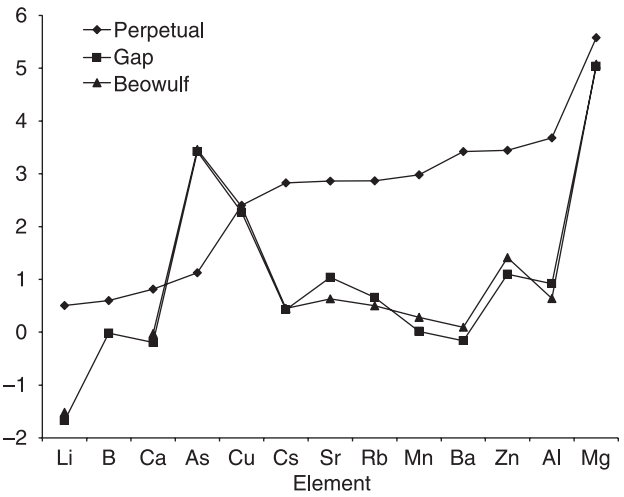

Fig. 3 Elemental concentration factors for hydrous ferric oxide surfaces relative to spring water (log ([surface]/[stream]) from three different springs.

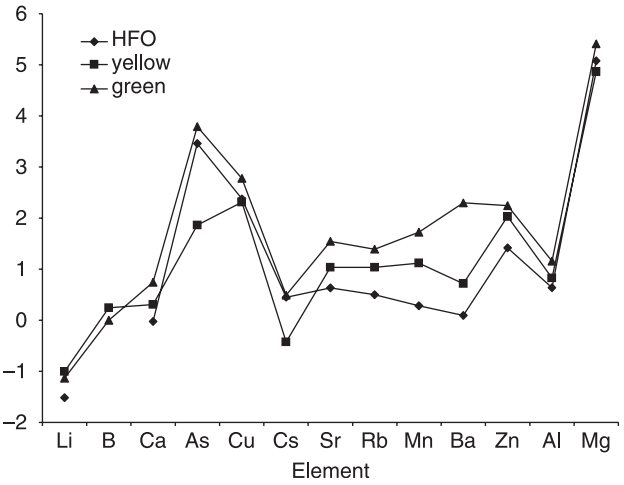

Fig. 4 Elemental concentration factors for hydrous ferric oxide (HFO) and microbial mat surfaces relative to spring water (log [surface]/[stream]) for the sampling sites within Beowulf Spring.

Substrate surface charge

Excess surface charge, as evaluated by right-hand side of equation (5), and normalized to sample dry weight, is presented in Fig. 5. At any given point, excess charge is equivalent to the cumulative surface concentration of deprotonated FGs, and

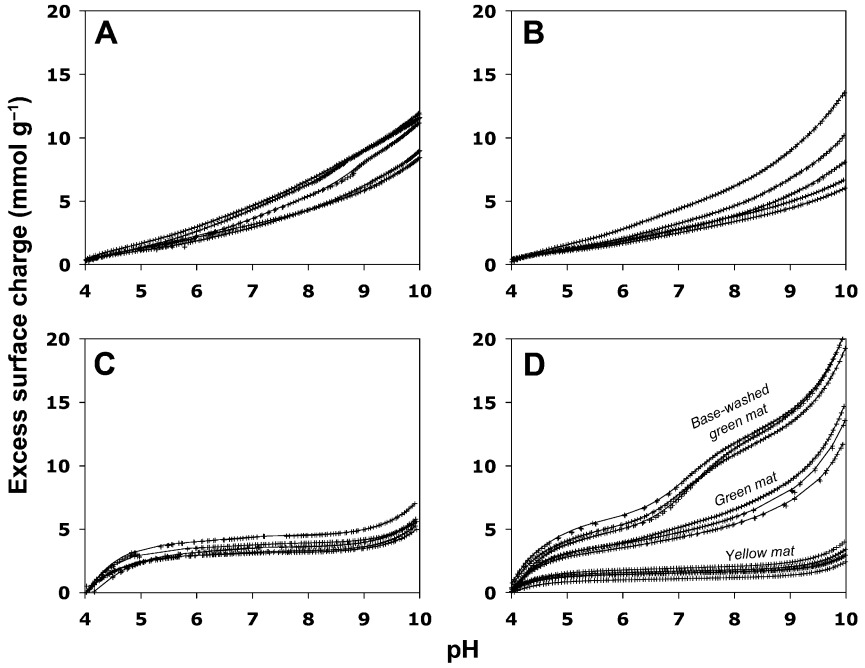

Fig. 5 Plots of excess surface charge associated with hydrous ferric oxide samples from: (A) Beowulf Spring; (B) Gap Spring; (C) Perpetual Spouter; and (D) samples of the yellow S^0-rich and the green *Cyanidia* mats from Beowulf Spring. All replicates are plotted together (n = 3 or n = 5). Data points represent excess charge data measured during titration and solid lines represent the excess charge calculated to arise from the set of functional groups modelled after each titration (the model goodness-of-fit).

the slope of the excess charge plot is the surface buffering capacity. For presentation purposes, excess surface charge plots were adjusted to zero at pH 4, and because the ANC term fitted by the pK_a spectrum modelling approach serves as a constant offset, the FGs modelled from titration data depend solely on the shape of the curve, and are thus independent of the apparent point of zero charge (see methods). All of the titration data are presented in Fig. 5 for the qualitative comparison of charging behaviour between samples, and for a visual indication of titration repeatability. Also included in Fig. 5 is the excess surface charge calculated from the set of FG concentrations that were fit to the measured excess surface charge data (i.e., from the left side of equation (5)), indicating the model goodness of fit for each replicate.

HFO obtained from the ASC springs (Beowulf and Gap Spring, Fig. 5A, and 5B, respectively) show comparable pH-dependent charging behaviour, with increased buffering capacity towards higher pH, as previously noted for synthetic HFOs (Dzombak and Morel, 1990). In contrast, HFO from the NC spring, Perpetual Spouter (Fig. 5C), displays charging behaviour that is largely static across the titration range, and the increased buffering capacity is noticeably absent until pH ~10. In other words, while the charging behaviour of HFO from ASC springs indicates relatively significant concentrations of FGs that deprotonate at circumneutral pH, the HFO from the NC spring indicates a lack of such sites. Discrete site modelling (discussed below) enables the quantification and direct comparison of such differences that are only visually inferred from excess charge data.

Excess charge plots representing Beowulf biomass are shown in Fig. 5D. The yellow mats display low reactivity over the entire titration range. In contrast, the green mats display significant surface reactivity, and similar to HFO samples from ASC springs, show increased buffering capacity at alkaline pH. It is critical to note that the green mat samples were split and prepared in two different ways: (1) the curves labelled 'green mat' correspond to samples that were rinsed at spring pH and ionic strength to examine the surfaces under conditions as close as possible to their *in situ* state, while (2) the 'base-washed' green mat samples were washed at alkaline pH to release any surface-complexed elements, and accordingly, better reflect surface charging inherent to the native microbial surface. 'Base-washed' green mat samples display charge profiles that are largely consistent with their unwashed counterparts at low pH, but display relatively increased reactivity at higher pH. In fact, sharp inflection in the former's excess charge curves at pH ~7 indicates a high concentration of sites with apparent pK_a values around 7.

Discrete site modelling

FG distributions for the HFO samples, modelled from the excess charge curves presented above, and composited over all replicates, are presented in Fig. 6. The HFOs from ASC springs (Beowulf and Gap, Fig. 6A and 6B, respectively) show FGs that are broadly consistent in pK_a distribution (e.g., four main sites) and in the relative concentrations of sites. Conversely, the HFOs from Perpetual Spouter show a FG distribution that is noticeably different; although it too has four main sites, they are noticeably less important at high pH, and the dominant site is an apparently acidic FG, suggestive of an apparent point of zero charge < 7 (Fig. 6C).

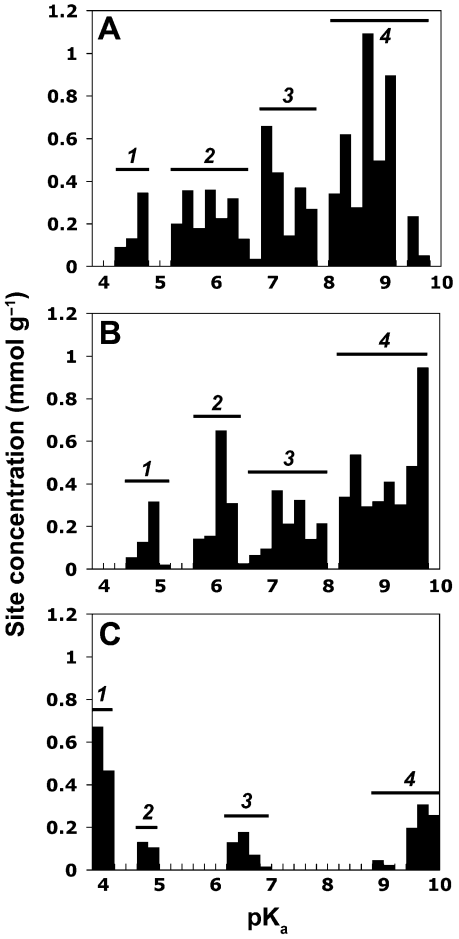

Fig. 6 Modelled functional group (FG) distributions for hydrous ferric oxide samples: (A) Beowulf Spring, (B) Gap Spring, and (C) Perpetual Spouter. For this composite plot, FG concentrations were summed over all five replicates at each pK_a interval and then normalized to total weight titrated. Individual surface FG types are identified by number for summary in Table 3.

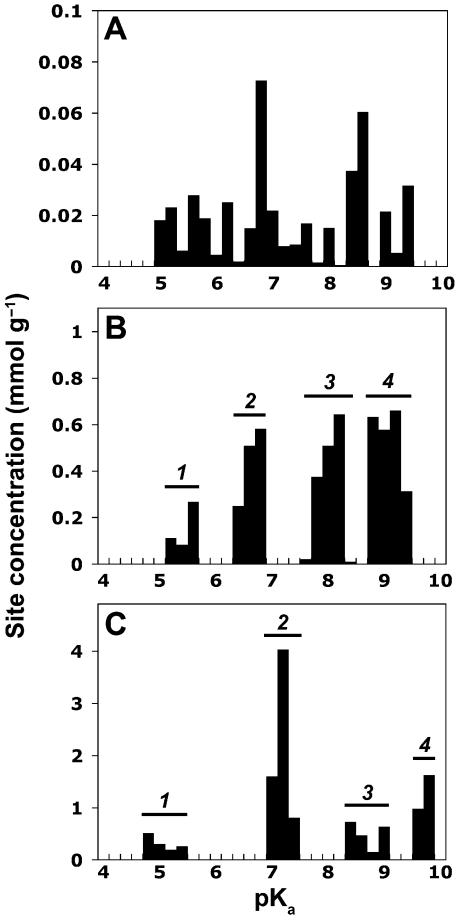

Fig. 7 Modelled functional group distribution for other microbial mat samples from Beowulf Spring: (A) green mat, (B) base-washed green mat, and (C) yellow mat. For this composite plot, FG site concentrations were summed over all five replicates at each pK_a interval and then normalized to total weight titrated. Individual surface FG types are identified by number for summary in Table 3.

FG distributions for microbial substrata are presented in Fig. 7. The yellow mats show a low density of FGs (note different y-axis increments), with a more or less scattered distribution, and for this reason assignment of individual types of FGs was not attempted (Fig. 7A). Unwashed green mats (Fig. 7B) show three FGs of approximately equal concentration, and a fourth, more acidic type of lesser concentration. Base-washed green mats (Fig. 7C) show FG types 1, 3, and 4 that are largely consistent with acid-washed counterparts in both pK_a and concentration; however, the concentration of FG type 2 is increased ~8 fold, most likely by the desorption of surface complexes as a consequence of the base-washing procedure (see discussion).

We also evaluated the reversibility of protonation/deprotonation reactions for green-mat samples in order to ensure that cells were not irreversibly altered (i.e., by cell lysis) at high pH. We did so by titrating unwashed samples from pH 11 to 3 immediately following their titration from pH 3 to 11, without changing the titration electrolyte (and thus retaining all metals that may have hydrolysed and desorbed during the up titration). Presented in Fig. 8 is an example excess surface charge plot for up and down titrations of the same green mat sample (Fig. 8A), as well as the sites modelled independently from 'up' titration (Fig. 8B) and 'down' titration (Fig. 8C) data. Both titration directions show similar pH-dependent charging profiles, and the slightly decreased reactivity during 'down' titration may be attributable, in part, to decreased sensitivity introduced by dilution of the titration suspension as a consequence of titrant previously added during 'up' titration. Nonetheless, it is evident from Fig. 8 that deprotonation/protonation reactions were largely reversible by the methods utilized herein, and that cell lysis was not likely responsible for the changes observed after the base-washing of green mat samples.

FG parameters for all samples are summarized along with estimates of error in Table 3. For HFO samples, total FG

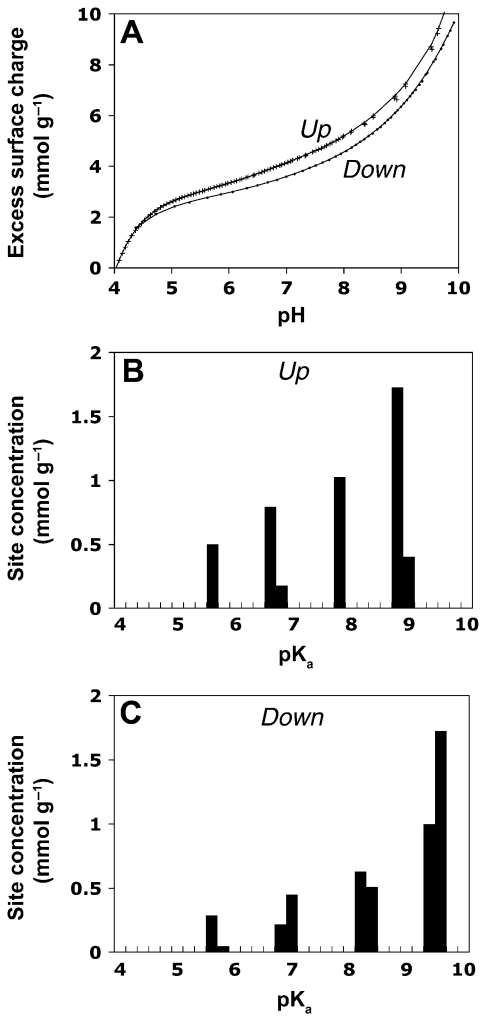

Fig. 8 Evaluating the reversibility of protonation/deprotonation reactions by reverse titration. (A) Surface charge plot showing reverse titration, where this sample (green mat from Beowulf Spring) was titrated up from 3 to 11, and then immediately back down to 3. The modelled site distributions for (B) up titration and (C) down titration show model sensitivity, as well as an indication of the data obtained from the modelling of a single titration.

concentrations were assessed as the sum of sites 1 and 2 combined with the average of sites 3 and 4, as we assume the latter represents the stepwise deprotonation of iron oxide surface sites (i.e., $>FeOH_2^+ \rightarrow >FeOH \rightarrow >FeO^-$, where '>' denotes the parent compound). The HFO samples from ASC springs show elevated total site concentrations (5.44 mmol g^{-1} and 4.63 mmol g^{-1} for Beowulf and Gap springs, respectively) relative to the Perpetual Spouter HFO (2.16 mmol g^{-1}). They also contain abundant FGs with high pK_a values, while the Perpetual Spouter HFO is deficient in such sites; correspondingly, the ASC HFOs are characterized by high apparent point of zero charge (PZC) values (7.59 and 7.87 for Beowulf and Gap Spring, respectively), while the Perpetual Spouter shows a lower apparent PZC of 6.21. The biomass samples also showed high apparent PZC values (ranging from 7.25 to 7.87), but varied

Table 3 Individual functional group pK_a values and concentrations for all samples investigated. Uncertainty is given as 2 standard error ($P = 0.05$) where available. Apparent point of zero charge (PZC) represents the pK_a value where the modelled concentration of sites is equal on both sides of the pK_a spectrum. Note that for hydrous ferric oxide (HFO) sites, the total concentration depends on presumed site identities (see text). Synthetic HFO data (sites 2 through 5 only) from Smith and Ferris (2001)

	pK_a					Concentration (mmol g^{-1})				
	Site 1	Site 2	Site 3	Site 4	Apparent PZC	Site 1	Site 2	Site 3	Site 4	Total
HFO Beowulf	4.61 ± 0.17	5.96 ± 0.23	7.34 ± 0.29	8.86 ± 0.15	7.59 ± 0.12	0.58 ± 0.37	1.83 ± 0.31	1.92 ± 0.44	4.14 ± 1.08	5.44 ± 0.92
HFO Gap Spring	4.98 ± 0.12	6.21 ± 0.03	7.45 ± 0.07	9.27 ± 0.20	7.87 ± 0.33	0.57 ± 0.19	1.40 ± 0.47	1.51 ± 0.38	3.80 ± 1.54	4.63 ± 1.24
HFO Perpetual Spouter	4.10 ± 0.04	5.20 ± 0.57	6.59 ± 0.14	9.63 ± 0.30	6.21 ± 1.76	1.33 ± 2.60	0.21 ± 0.29	0.41 ± 0.14	0.84 ± 0.45	2.16 ± 2.39
Synthetic HFO	4.78 ± 0.34	5.73 ± 0.50	7.32 ± 0.44	8.75 ± 0.37	nd	0.34	0.37	0.30	1.06	2.42
Green mat	5.43 ± 0.24	6.65 ± 0.03	8.00 ± 0.23	9.03 ± 0.24	7.87 ± 0.29	0.46 ± 0.09	1.37 ± 0.65	1.59 ± 0.59	2.17 ± 0.88	5.59 ± 0.98
Base-washed green mat	5.11 ± 0.32	7.17 ± 0.10	8.64 ± 0.33	9.65 ± 0.17	7.72 ± 0.20	1.27 ± 0.56	6.46 ± 0.89	2.00 ± 0.45	2.57 ± 2.55	12.30 ± 1.94
Yellow mat	nd	nd	nd	nd	7.25 ± 0.40	nd	nd	nd	nd	0.52 ± 0.13

nd, not determined.

considerably in their total FG concentration. For instance, the yellow mat possesses a low total FG concentration of 0.52 mmol g^{-1}, while the green mat had an order of magnitude more FGs (5.59 mmol g^{-1}), which more than doubles (to 12.30 mmol g^{-1}) as the result of the base-washing procedure. As was mentioned in the methods, we define apparent PZC as the mean of site pK_a values weighted by their concentration (apparent PZC, see Table 3), as compared to a true PZC, which is defined as the pH where surface charge is zero. The difference herein lies in the fact that we could not measure sites of extreme pK_a, as well as sites that may have retained adsorbed surface complexes throughout titration. This explains the discrepancy between previous studies showing PZC values of microbial cell surfaces between 2 and 4 (Harden and Harris, 1953) and our results.

DISCUSSION

HFO surface reactivity

HFOs from both ASC springs (Beowulf and Gap) are characterized by an abundance of FGs at pK_a 7 and 9, ascribed to the first and second stepwise deprotonation of iron-oxyhydroxide hydroxyl groups. Actually, these HFOs closely mimic pure synthetic HFO with respect to FG site concentrations, pK_a distribution (Smith and Ferris, 2001), and high PZC (e.g., 8.8, Sverjensky and Sahai, 1996). In contrast, the NC spring (Perpetual Spouter) HFO is largely dominated by a low pK_a FG (4.1) and, correspondingly, has a lower apparent PZC of 6.2. Although we cannot be absolutely confident as to why differences in apparent PZC exist between the HFOs from ASC and NC springs, the most noticeable difference in HFO composition is the amount of silica associated with these solids. For example, HFOs from Beowulf and Gap Spring have low to undetectable silica contents, whereas the HFOs from Perpetual Spouter contain up to 78% SiO_2 by weight (W. P. Inskeep, personal communication). Silica incorporation into HFO is important because previous studies have shown that it effectively lowers the PZC to values between 5–7 (Schwertmann and Fechter, 1974). Thus far, no studies that we are aware of have described the characteristics of silica-rich HFO in terms of FG site distribution, but we find that in the NC system, HFO hydroxyl site concentrations are considerably lower, presumably as a result of solid phase silica (detrital quartz or authigenic amorphous silica) 'diluting' the concentration of the available HFO sites, or alternatively, dissolved silica reacting with Fe resulting in HFO surface sites whose chemical nature is distinct from the individual components. Although all springs investigated possess similar dissolved silica concentrations (recall Table 1), the fact that protons appear to inhibit the polymerization of silica (Fournier, 1985), and at low pH, amorphous silica has a more neutral surface charge (PZC ~2; Parks, 1965), may explain the absence of silica in the ASC HFOs.

The PZC values of the HFOs have an important bearing on sorption reactions taking place at the mineral–water interface. HFOs from the ASC springs are in equilibrium with waters at pH <3, and consequently, an apparent PZC of 7.6–7.9 means that their surfaces will remain positively charged. This facilitates the electrostatic adsorption and surface complexation of dissolved anions. In the ASC springs, arsenate ($H_2AsO_4^-$) is highly concentrated by the HFOs as the result of edge and corner sharing bidentate binuclear and bidentate mononuclear As(V) complexation to hydroxyl groups of Fe(III) (Inskeep *et al.*, 2004). However, Fe(III) hydroxyl FGs with pK_a 7–9 are noticeably absent for HFO from Perpetual Spouter. The apparent PZC of these HFO surfaces is 6.2, less than the pH of the waters to which these surfaces are exposed (7.0). Unlike the ASC HFOs, the NC HFO surfaces will be negatively charged, and indeed, they are more reactive to dissolved cations (see Table 2). For example, Al, Ba, Ca, Cs, Li, Mn, Sr, Rb, and Zn are found in concentrations that are an order of magnitude higher than on the ASC HFO. Conversely, the concentration of arsenate is an order of magnitude lower than on ASC HFO surfaces. These results clearly demonstrate the importance of surface chemical functional groups, and the surface charge they confer, for solute adsorption in these hydrothermal systems.

Microbial surface reactivity

Surface reactivity varies considerably between the two different microbial communities associated with Beowulf Spring. SEM images show that the yellow mat consists of filamentous microorganisms within a matrix of amorphous and rhombohedral S° (Langner *et al.*, 2001; Macur *et al.*, 2004). Our results indicate that the yellow mats have a surface reactivity (0.52 mmol g^{-1} summed over the titration range) that is comparable to previously reported values for thermophilic bacteria (e.g., 0.85 mmol g^{-1}, Burnett *et al.*, 2006), but lower than values reported for mesophilic bacterial cultures (averaging 3.2 ± 1.0 mmol g^{-1}, after Borrok *et al.*, 2005, and assuming a 10:1 wet-to-dry weight ratio for the purposes of comparison). The lower surface reactivity of the yellow mats may be due to (i) an inherent quality of thermophilic cell surfaces; (ii) the low reactivity of elemental sulfur during titration; and/or (iii) possibly a relatively high weight ratio of EPS to cells. In the case of the latter scenario, EPS may not contribute excess charge within our titration range as it can be dominated by hydrated polysaccharides rich in hydroxyl functional groups that deprotonate at pH values greater than 10 (Liu and Fang, 2002).

Green mats sampled at Beowulf are dominated by *Cyanidia* algae (Jackson *et al.* 2001). Unlike other samples, surface properties of the green mats were determined by titration following two different preparation procedures; (1) rinsing at stream pH and ionic strength to leave natural sorbates intact on the algal surfaces, and (2) washing at pH 11 to strip the sorbates and better reveal native FGs on the cell surfaces. Our results show that both unwashed and washed FG concentrations

(5.59 mmol g^{-1} and 12.30 mmol g^{-1} dry weight, respectively; Table 2) are not only higher than the yellow mats, but they are also higher than total FG concentrations determined for other eukaryotes; e.g. the alga *Pseudokirchneriella subcapitata* (~0.4 mmol g^{-1} dry weight from pH 3 to 10, Kaulbach *et al.*, 2005) and the fungus *Saccharomyces cerevisiae* (~1.4 mmol g^{-1}, Naeem *et al.*, 2006) (note: we assume a wet to dry weight ratio of 10:1 for the purpose of these comparisons). Indeed, our values are considerably higher than previously reported for any microbial surface. With that said, our samples likely contain a heterogeneous mixture of intact cells, cellular debris, and cells that lysed during wash at pH 11; the latter two would expose additional FGs not associated with cell surface layers.

Unlike most bacteria that possess an abundance of FGs with low pK_a (generally attributed to carboxyl groups; e.g., Beveridge and Murray, 1976; Jiang *et al.*, 2004), such FGs are found in low concentration for *Cyanidia* (Fig. 7B, C). Instead, the algal surfaces appear dominated by FGs with pK_a values above 5, leading to an apparently high PZC. Based on the organic acid protonation constants from Martell and Smith (1989), we attribute site 1 to carboxyl groups, site 2 to phosphate groups, site 3 to phosphate or amino groups, and site 4 to amino groups. It is interesting that sites 1, 3, and 4 remained unchanged by the washing procedure; not only does this imply that they represent organic surface sites, but that any elements released into solution during the titration of unwashed samples had a negligible effect on modelled FG site concentrations (Fig. 7A vs. 7B). By comparison, there was a nearly ~5-fold increase in the concentration of site 2 as the result of the pH 11 washing procedure.

The washing procedure also resulted in the desorption of a range of elements, in particular Mg and As (see Table 2). The changes in site 2 and the release of Mg and As suggests that these elements were bound to that FG. Certainly, the concentration of site 2 FGs that were revealed by washing can more than quantitatively account for the whole of Mg and As adsorption. The association of Mg with cell surfaces may not be unsurprising given that previous findings have shown that Gram-positive bacteria utilize it to cross-link phosphate residues associated with teichoic acid molecules, and in doing so, eliminate the repulsive anionic charges between adjacent molecules, giving rise to more dense but stable structures (Doyle *et al.*, 1974). In Gram-negative bacteria, calcium functions in a similar manner, bridging adjacent molecules of LPS together and anchoring the outer membrane to the underlying peptidoglycan layer (Ferris and Beveridge, 1986). At present, information regarding *Cyanidia* surface ultrastructure is insufficient for us to conclude with any level of certainty whether the adsorbed Mg here serves a similar function. With regard to As, its association is unexpected because of its anionic nature. Although the FG responsible for As(V) sorption may have a pK_a that lies outside of the titration range, it is also possible that Mg serves as a cation bridge between phosphate FGs and arsenic oxyanions. In fact, magnesium oxides and hydroxides have been patented for use in As(V) sequestration from drinking water supplies (United States Patent 6821434). Additional spectroscopic methods, as described above, would be required to confirm the nature of the algal As(V) surface complexes.

Surface complexation modelling

The main goal of this study was to evaluate and compare the natural surface reactivity of hydrothermal HFOs and microbial communities. The surface chemical data presented herein is directly applicable to surface complexation models designed to account for ion sorptive behaviour as a function of temperature, ionic strength, and sorbent to sorbate ratio. These models predict adsorption equilibrium by considering the formation of surface complexes to be governed by mass-action equations. Additionally, surfaces that are charged possess electrical potential gradients that may strongly influence sorption reactions by the energy required to move ions against those gradients, and the various surface complexation models (e.g., constant capacitance, triple-layer, etc.) differ in the mathematical representation of these electrical potential gradients. For example, the diffuse-layer model presupposes that all adsorbed ions occupy the same surface plane, and that the charge associated with that surface is balanced by charge associated with aqueous counter ions positioned in a diffuse layer that forms the boundary between the surface and the aqueous phase. The energy associated with moving an ion from the bulk solution to the surface, with or against the electrical potential gradient, is accounted for by a change in apparent ion activity, as determined by an exponential Boltzmann expression:

$$(X_s^z) = (X^z)[e^{-\psi F/RT}]^z \quad (7)$$

where the surface activity (X_s^z) of ion X with charge z is related to the activity of X in solution (X^z) by the unitless Boltzmann factor $e^{-\psi F/RT}$ considering surface potential (ψ), Faraday constant (F), ideal gas constant (R), and absolute temperature (T) (Langmuir, 1997).

These models require prior knowledge of all potential surface complexes, their intrinsic stability constants, and chemical and electrical parameters describing the surface of interest. At present, there is a paucity of stability constants describing metal sorption to microbial surfaces, although methods have been proposed to extrapolate microbial surface stability constants from stability constants describing aqueous complexation between elements and analogous organic acids (Fein *et al.*, 2001). Fortuitously, many proton and metal stability constants have been previously determined for HFO surface FGs, and surface complexation models have extensively applied to synthetic HFO surfaces (Dzombak and Morel, 1990). In this study, we use our experimentally determined surface chemical parameters, along with literature metal-HFO stability constants,

to test the ability of the SCM to describe metal sequestration by natural HFOs.

In order to apply a diffuse-layer SCM, several important assumptions regarding the nature of our HFO samples were required:

(i) For modelling purposes, and as discussed previously, FG types 3 and 4 represent the stepwise deprotonation of $>FeOH_2^+$; thus the concentration of iron surface sites were taken as an average of FG types 3 and 4, and their intrinsic proton stability constants were replaced in the Visual MINTEQA2 HFO sorption database by their apparent proton stability constants determined in this study by titration.

(ii) FG types 1 and 2 correspond to surface moieties of an Fe-As oxyhydroxide, and their apparent proton stability constants were assumed to represent the deprotonation from >(Fe,As)OH to >(Fe,As)O^-. No data exist pertaining to sorption reactions involving such ligands, and for modelling purposes, the stability constants of surface complexes compiled for HFO were assigned to these putative species. As discussed below, these FGs must be accounted for in order to explain the observed elemental partitioning to the As-rich HFO surfaces.

(iii) The relative concentration of surface FGs vs. solutes is very low on a per-litre basis in all hydrothermal springs investigated. This assumption allows for consideration of the rapidly moving stream water with which the HFO surfaces are in contact; as stream water is in contact with a given surface for only a short period, the adsorption of ions to the HFO surface should not deplete their aqueous concentration in stream water. In other words, to avoid the depletion of solutes in our model, we assume that a rapidly flowing stream is equivalent to a large volume of water with which the HFO surface is in contact. As long as this assumption is valid, other competing sorbents (such as bacteria, algae, other mineral phases, DOC, etc.) will also have negligible effect on stream water composition, and thus may be considered as systems separate to that of the HFO–water interface.

(iv) The surface area of the HFO is similar to that of synthetic HFO (600 $m^2\ g^{-1}$, Roden *et al.*, 2003), and that there existed no difference in surface area between the various HFO samples. We consider this assumption a potentially large source of error; however, due to the solid nature of the HFO mats and the homogenization required for analysis, independent assessments of mineral surface area were not possible.

The predicted and measured surface concentrations of various ions for all three HFOs are presented in Fig. 9 (note that cesium, lithium, and rubidium species could not be considered in the model due to a lack of thermodynamic data describing their affinity for the HFO surface). The plots are organized such that (1) surface FG site concentrations that are under-predicted by the model are found at the left-hand side, (2) the surface FG site concentrations that are over-predicted by the model are found on the right-hand side, and (3) the best fit is found about the center.

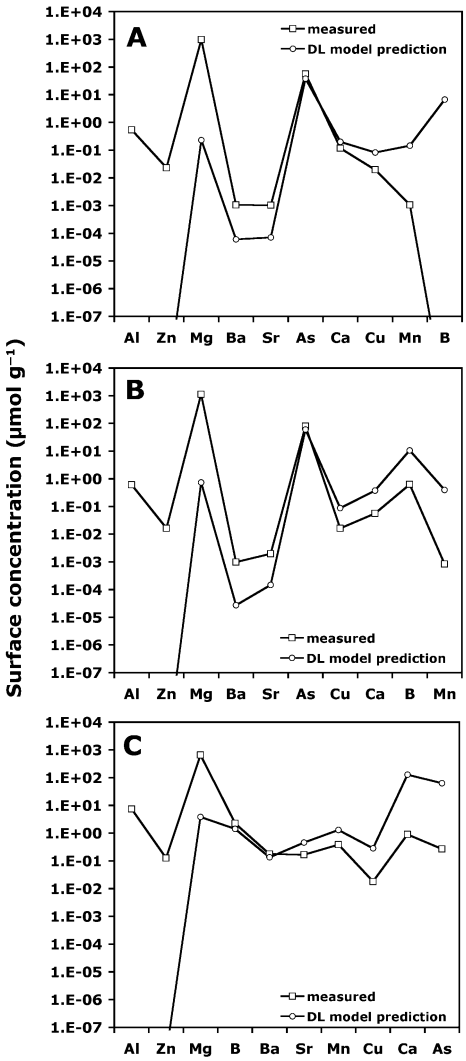

Fig. 9 Measured surface ion concentrations associated with HFOs compared to those predicted by diffuse-layer surface complexation modelling. Elements are ordered according to their degree of under- or over-prediction. (A) Beowulf Spring, (B) Gap Spring, and (C) Perpetual Spouter Spring.

The HFOs from the ASC springs, Beowulf and Gap Spring (Fig. 9A,B, respectively), show similar predicted and measured surface FG concentrations. In both cases, the sorption of As is well accounted for by the surface properties of the HFOs, as determined by discrete site modelling; the sorption of arsenate is predicted to occur onto positively charged $>FeOH_2^+$ sites (represented by FG types 3 and 4 in Fig. 6), and these sites, being fully protonated at stream pH in both ASC springs, do not contribute to the sorption of cationic species. Meanwhile, the adsorption of cations is dependent on assumption (ii) that the sites of lower pK_a (FG types 1 and 2, Fig. 6) deprotonate from a neutral state to a negative one, and consequently, a small proportion (predicted from pK_a and concentration data by SCM) will remain deprotonated at the low stream pH and

present negatively charged reactive sites for the sorption of cations. Accordingly, surface complexation modelling predicts that FG types 1 and 2 are responsible for the bulk of cation complexation. The breakdown of the model in Fig. 9A,B on either side of arsenic can be attributed to the differences in the previously determined affinity of synthetic HFO sites and the true affinity of Fe-As oxyhydroxide sites for available cations. Therefore, assumption 2, whereby such FGs are presumed to have a similar affinity for aqueous cations as HFO sites, is invalid. The model thus demonstrates that while the As-rich HFOs from ASC springs possess $>FeOH_2^+$ surface FGs that fully account for the adsorption of arsenic, the presumed Fe-As sites differ in affinity for aqueous cations, with Al, Zn, Mg, Ba, and Sr having a higher affinity for a fully deprotonated Fe-As site than a fully deprotonated FeO^- site, and for B, Mn, Cu, and Ca, the reverse is true.

In the case of the NC spring, the above assumptions become even less valid; Perpetual Spouter has abundant silica in the solid phase, and as a result, the concentration of surface FGs that may be compared with synthetic HFO (such as types 3 and 4 in the case of ASC springs) is noticeably reduced. The sorption of arsenic should occur with strong preference to $>FeOH_2^+$ sites, as exemplified in Fig. 9A,B. However, in the case of Perpetual Spouter, arsenic is the surface species most over predicted by SCM (Fig. 9C). The predicted surface arsenic concentration is calculated using the concentration of Fe sites as determined by titration, and the Fe sites presumed to be present on the HFO from Perpetual Spouter should have bound more arsenic than was measured there. Unlike ASC springs, where discrepancies were solely attributed to the different affinities of cations to Fe and (Fe,As) surface sites, the deviation of Perpetual Spouter from the model likely results from the significant presence of silica, although some FG sites attributable to silica may fall outside of the titration range and therefore cannot be included in SCM. As discussed above, silica will serve to lower the PZC of the solid from Perpetual Spouter and electrostatically inhibit the sorption of arsenic, as appears to be the case with the HFO samples. Similarly, surface complexes of Mg (as well as Al and Zn) that are under-predicted by the model have a high affinity for silica, and although they are undetectable by titration, silica surface sites also possibly account for the sorptive behaviour of these dissolved species.

Finally, although the adsorption of metals occurred while the substrates were submerged at temperatures ranging from ~80 to ~50 °C, depending on the spring, modelling was performed using functional group concentrations, proton stability constants, and literature thermodynamic data based on 25 °C. Although the temperature dependence of proton adsorption may be minimal in the case of microbial surfaces (Wightman *et al.*, 2001), and metal adsorption slightly more dependant on temperature (Gorman-Lewis *et al.*, 2006), the effect of temperature on HFO protonation and metal sorption could not be tested at present with the SCM employed here.

CONCLUSIONS

In ASC springs, HFO and green *Cyanidia* algae have similar overall reactivity, and display comparable elemental sorption patterns, despite possessing FGs that differ in chemical composition, site concentration, and pK_a distribution, whereas yellow S^o-encrusted mats possess significantly lower overall reactivity. These findings highlight the fact that sorptive properties may vary between different microbial populations in close proximity. We also show that HFO from a NC spring bound significantly more cations, but less arsenic, than ASC HFOs, a pattern coincident with a lower apparent PZC and a high solid-phase silica content. The additional application of diffuse-layer surface complexation modelling to the HFO samples suggests that iron-arsenic oxyhydroxide (ASC springs) or silica (NC springs) sites are responsible for the majority of cation adsorption at such low pH conditions. Overall, these results highlight the importance of chemical parameters, such as surface functional group concentrations and pK_a distributions, in accounting for complex sorption phenomena. While surface complexation modelling could, at present, only be applied to the HFO samples, it is assumed that a similar approach may eventually be achieved for microbial biomass, and ultimately, facilitate a better understanding of the microbial role in elemental partitioning in natural systems.

ACKNOWLEDGEMENTS

This research was supported by a Natural Sciences and Engineering Research Council award to KK (249565-2002). WPI and TRM appreciate support from the US National Aeronautics and Space Administration (NAG5-8807, NNG04GR46G), the US National Science Foundation (MCB-0132022), and the Montana Agricultural Experiment Station (Projects 911398 and 911310). The work contained herein was performed under Research Permit no. YELL-2005-SCI-5068, and the authors appreciate permitting assistance from C. Hendrix (Yellowstone Center for Resources). We would also like to thank three anonymous reviewers for their insightful comments.

REFERENCES

Ball JW, McCleskey RB, Nordstrom DK, Holloway JM, Verplanck PL (2002) *Water-Chemistry Data for Selected Springs, Geysers, and Streams in Yellowstone National Park, Wyoming 1999–2000.* United States Geological Survey Open File Report 02-382, Boulder, Colorado.

Bayer ME, Sloyer Jr, JL (1990) The electrophoretic mobility of gram-negative and gram-positive bacteria: an electrokinetic analysis. *Journal of General Microbiology* **136**, 867–874.

Bethke CM, Brady PV (2000) How the Kd approach undermines ground water cleanup. *Ground Water* **38**, 435–443.

Beveridge TJ, Murray RGE (1976) Uptake and retention of metals by cell walls of *Bacillus subtilis*. *Journal of Bacteriology* **127**, 1502–1518.

Borrok D, Turner BJ, Fein JB (2005) A universal surface complexation framework for modeling proton binding onto bacterial surfaces in geological settings. *American Journal of Science* **305**, 826–853.

Brassard P, Kramer JR, Collins PV (1990) Binding site analysis using linear programming. *Environmental Science and Technology* **24**, 195–201.

Cox JS, Smith DS, Warren LA, Ferris FG (1999) Characterizing heterogeneous bacterial surface functional groups using discrete affinity spectra for proton binding. *Environmental Science and Technology* **33**, 4514–4521.

Davis JA, Kent DB (1990) Surface complexation modeling in aqueous geochemistry. In *Reviews in Mineralogy Vol 23: Interface Geochemistry*. Hochella MF, White AF (eds). Mineralogical Society of America, Washington, DC, pp. 177–248.

Donahoe-Christiansen J, Jackson CR, D'Imperio S, Inskeep WP, McDermott TR (2004) Arsenite-oxidizing *Hydrogenobaculum* sp. isolated from an acid-sulfate-chloride geothermal spring in Yellowstone National Park. *Applied and Environmental Microbiology* **70**, 1865–1868.

Doyle RJ, McDannel ML, Streips UN, Birdsell DC, Young FE (1974) Polyelectrolyte nature of bacterial teichoic acids. *Journal of Bacteriology* **118**, 606–615.

Dzombak DA, Morel FMM (1990) *Surface Complexation Modeling. Hydrous Ferric Oxide*. John Wiley and Sons, New York.

Fein JB, Daughney CJ, Yee N, Davis TA (1997) A chemical equilibrium model for metal adsorption onto bacterial surfaces. *Geochimica et Cosmochimica Acta* **61**, 3319–3328.

Fein JB, Martin AM, Wightman PG (2001) Metal adsorption onto bacterial surfaces: Development of a predictive approach. *Geochimica et Cosmochimica Acta*, **65**, 4267–4273.

Ferris FG, Beveridge TJ (1986) Physiochemical roles of soluble metal cations in the outer membrane of *Escherichia coli* K-12. *Canadian Journal of Microbiology* **32**, 594–601.

Fournier RO (1985) The behaviour of silica in hydrothermal solutions. In *Geology and Geochemistry of Epithermal Systems*, Berger BR, Bethke PM (eds). Society of Economic Geologists, El Paso, TX **2**, 45–61.

Gorman-Lewis D, Fein JB, Jensen MP (2006) Enthalpies and entropies of proton and cadmium adsorption onto *Bacillus subtilis* bacterial cells from calorimetric measurements. *Geochimica et Cosmochimica Acta* **70**, 4862–4873.

Gustafsson JP (2000) *Visual Minteq* [WWW document]. URL http://www.lwr.kth.se/English/OurSoftware/vminteq/ (verified 13 March 2006).

Harden VP and Harris JO (1953) The isoelectric point of bacterial cells. *Journal of Bacteriology* **65**, 198–202.

Hunt S (1986) Diversity of biopolymer structure and its potential for ion-binding applications. In *Immobilisation of Ions by Bio-Sorption*. Eccles H, Hunt S (eds). Ellis Harwood, Chichester, UK, pp. 15–46.

Inskeep WP, Macur RE, Harrison G, Bostick BC (2004) Biomineralization of As(V)-hydrous ferric oxyhydroxide in microbial mats of an acid-sulfate-chloride geothermal spring, Yellowstone National Park. *Geochimica et Cosmochimica Acta* **68**, 3141–3155.

Jackson CR, Langner HW, Donahoe-Christiansen J, Inskeep WP, McDermott TR (2001) Molecular analysis of microbial community structure in an arsenite-oxidizing acidic thermal spring. *Environmental Microbiology* **3**, 532–542.

Jiang W, Saxena A, Bongkeun S, Ward BB, Beveridge TJ, Myneni SCB. (2004) Elucidation of functional groups on Gram-positive and Gram-negative bacterial surfaces using infrared spectroscopy. *Langmuir* **20**, 11433–11442.

Kaulbach EM, Szymanowski JES, Fein JB 2005. Surface complexation modelling of proton and Cd adsorption onto an algal cell wall. *Environmental Science and Technology* **39**, 4060–4065.

Kennedy CB, Martinez RE, Scott SD, Ferris FG (2003) Surface chemistry and reactivity of bacteriogenic iron oxides from Axial Volcano, Juan de Fuca Ridge, north-east Pacific Ocean. *Geobiology* **1**, 59–70.

Konhauser KO (1998) Diversity of bacterial iron mineralization. *Earth-Science Review* **43**, 91–121.

Konhauser KO (2007) *Introduction to Geomicrobiology*. Blackwell Publishing, Oxford, UK.

Langner HW, Jackson CR, McDermott TR, Inskeep WP (2001) Rapid oxidation of arsenite in a hot spring ecosystem, Yellowstone National Park. *Environmental Science and Technology* **35**, 3302–3309.

Langmuir D (1997) *Aqueous Environmental Geochemistry*. Prentice Hall, Upper Saddle River, New Jersey.

Liu H, Fang HP (2002) Characterization of electrostatic binding sites of extracellular polymers by linear programming analysis of titration data. *Biotechnology and Bioengineering* **80**, 806–811.

Macur RE, Langner WH, Kocar BD, Inskeep WP (2004) Linking geochemical processes with microbial community analysis: successional dynamics in an arsenic-rich, acid-sulphate-chloride geothermal spring. *Geobiology* **2**, 163–177.

Martell AE, Smith RM (1989) *Critical Stability Constants*. Plenum Press, New York.

Morin G, Juillot F, Casiot C, Bruneel O, Personné JC, Elbaz-Poulichet F *et al.* (2003) Bacterial formation of tooeleite and mixed arsenic (III) or arsenic (V) – iron (III) gels in the Carnoulès acid mine drainage in France: a XANES, XRD, and SEM study. *Environmental Science and Technology* **37**, 1705–1712.

Naeem A, Woertz JR, Fein JB (2006) Experimental measurement of proton, Cd, Pb, Sr, and Zn adsorption onto the fungal species *Saccharomyces cerevisiae*. *Environmental Science and Technology* **40**, 5724–5729.

Parks, GA (1965) The isoelectric points of solid oxides, solid hydroxides, and aqueous hydroxo complex systems. *Chemical Reviews* **65**, 177–198.

Roden EE (2003) Fe(III) oxide reactivity toward biological versus chemical reduction. *Environmental Science and Technology* **37**, 1319–1324.

Schwertmann U and Fechter H (1982) The point of zero charge of natural and synthetic ferrihydrites and its relation to adsorbed silicate. *Clay Minerals* **17**, 471–476.

Seckbach J (1994) The natural history of *Cyanidium* (Geitler 1933): past and present perspectives. In *Evolutionary Pathways and Enigmatic Algae: Cyanidium caldarium (Rhodophyta) and Related Cells*. Seckbach J (ed.). Kluwer Academic Publishers, Dordrecht, the Netherlands, pp. 99–112.

Smith DS, Ferris FG (2001) Proton binding by hydrous ferric oxide and aluminium oxide surfaces interpreted using fully optimized continuous pKa spectra. *Environmental Science and Technology* **35**, 4637–4642.

Smith DS and Ferris FG (2003) Specific surface chemical interactions between hydrous ferric oxide and iron reducing bacteria determined using pK spectra. *Journal of Colloid and Interface Science* **266**, 60–67.

Sverjensky DA, Sahai N (1996) Theoretical prediction of single-site surface-protonation equilibrium constants for oxides and silicates in water. *Geochimica et Cosmochimica Acta* **60**, 3773–3797.

Waychunas GA, Rea BA, Fuller CC, Davis JA (1993) Surface

chemistry of ferrihydrite: Part 1. EXAFS studies on the geometry of coprecipitated and adsorbed arsenate. *Geochimica et Cosmochimica Acta* **57**, 2251–2269.

Wightman PG, Fein JB, Wesolowski DJ, Phelps TJ, Benezeth P, Palmer DA (2001) Measurement of b acterial surface protonation constants for two species at elevated temperatures. *Geochimica et Cosmochimica Acta* **65**, 3657–3669.

Yee N, Fein JB (2001) Cd adsorption onto bacterial surfaces: A universal adsorption edge? *Geochimica et Cosmochimica Acta* **65**, 2037–2042.